Nanoscale

PAPER

View Article Online
View Journal | View Issue

Cite this: *Nanoscale*, 2018, **10**, 8628

The comparative effect of wrapping solid gold nanoparticles and hollow gold nanoparticles with doxorubicin-loaded thermosensitive liposomes for cancer thermo-chemotherapy†

Yanan Li, ‡[a] Dongsheng He, ‡[a] Jiasheng Tu,‡[a] Ru Wang,[a] Chang Zu,[a] You Chen,[a] Wenqian Yang,[a] Di Shi,[b] Thomas J. Webster *[b] and Yan Shen*[a]

Received 6th December 2017,
Accepted 10th March 2018

DOI: 10.1039/c7nr09083h

rsc.li/nanoscale

Since conventional chemotherapy is a systemic treatment that affects the body globally and will not concentrate inside the tumor, it causes adverse side effects to patients. In this study, doxorubicin (DOX) together with solid gold nanoparticles (GNPs) or hollow gold nanoparticles (HGNPs), respectively, is loaded inside thermosensitive liposomes (GNPs&DOX-TLs and HGNPs&DOX-TLs), where the GNPs and HGNPs act as a "nanoswitch" for killing tumor cells directly by hyperthermia and triggering DOX release from TLs in the tumor quickly by near infrared laser (NIR) illumination. In addition, this study investigated the photothermal transformation ability, NIR triggered drug release behavior, and the intracellular uptake and cytotoxicity of breast tumor cells and the thermo-chemotherapy mediated by the co-delivery of GNPs&DOX-TLs and HGNPs&DOX-TLs. GNPs and HGNPs had very different light-to-heat transduction efficiencies, while the hollow HGNPs had the advantage of NIR surface plasmon tunability, resulting in the photothermal ablation of tumors with 800 nm light penetration in tissue. The prepared HGNPs&DOX-TLs exhibited a spherical shape with a diameter of 190 nm and a ξ potential of −29 mV, which were steadily dispersed for at least one month. The co-encapsulated DOX was released under hyperthermia caused by NIR-responsive HGNPs and the local drug concentration increased along with the disintegration of the liposomal membrane. This co-delivery of HGNPs&DOX-TLs produced a synergistic cytotoxicity response, thereby enhancing anticancer efficacy 8-fold and increasing the survival time compared to GNPs&DOX-TLs. This work suggested that the co-delivery of HGNPs&DOX-TLs followed by burst-release of DOX using NIR-responsive HGNPs sensitized cancer cells to the chemotherapeutic compound, which provided a novel concept for the combination strategy of chemotherapy and photothermal therapy. These results suggest that the markedly improved therapeutic efficacy and decreased systemic toxicity of the NPs presented in this study hold significant potential for future cancer treatment.

1. Introduction

Due to the complexity and heterogeneity of tumors,[1,2] the therapeutic efficiency of single-treatment methods such as surgical extirpation, chemotherapy, radiation therapy, or thermotherapy alone is limited.[3,4] Surgical extirpation is highly effective in primary tumors; however, it is limited to those that are surgically recognizable and accessible and thus cancer cells may not be completely removed. Chemotherapy commonly has significant negative side effects due to the drug toxicity to normal cells and is subject to the development of resistance by cancer cells.[5] Radiation, often used as a complementary approach to eradicate remaining cancer cells after surgery, can cause damage to the healthy tissue close to the cancer cells or in the path of the radiation beam. Moreover, because of absorption by normal tissues, the amount of energy deposited in the treatment volume is limited, which reduces the potency of the thermal killing effect. Therefore, combined therapy methods have become a focus in tumor treatment research.[6,7]

For clinically effective anticancer chemotherapy, selective drug delivery to the tumor needs to be further improved. Liposomes and other nanocarriers have been used for decades as anticancer devices because of their enhanced tumor per-

[a]*Department of Pharmaceutics, School of Pharmacy, China Pharmaceutical University, 24 Tong Jia Xiang, Nanjing, China. E-mail: shenyan@cpu.edu.cn*
[b]*Department of Chemical Engineering, Northeastern University, Boston, Massachusetts, 02115, USA. E-mail: th.webster@neu.edu*

†Electronic supplementary information (ESI) available. See DOI: 10.1039/c7nr09083h

‡These authors contributed equally to this work.

meability and retention (EPR) effect. Although liposomes have showed increased tumor accumulation and great stability *in vivo*, the release of drugs from liposomes was not controlled and was relatively slow, which resulted in the failure of anti-tumor therapy.[8–11] In order to overcome these challenges, stimuli-responsive drug delivery was introduced because of its site-selective ability, controlled-release pattern and enhanced therapeutic efficacy with reduced side effects. Stimuli-responsive drug delivery liposomes have attracted much attention and various triggering factors have been researched, for instance, the decreased pH in the tumor environment,[12] a specific enzyme,[13] light,[14] and ultrasound[15] for specific release of cargo drugs locally in the tumor.

Among them, thermosensitive liposomes (TLs) with a hyperthermia-triggered release mechanism have been fabricated and have demonstrated low cytotoxicity and stability under physiological conditions. The system consisted of heat-generating liposomes conjugated with gold nanoparticles, selected because of their unique optical properties.[16,17] Despite the remarkable advantages such as triggered release, potential challenges remain. The first challenge was to find a way to heat the liposomes to realize specific drug release. Drug release may be triggered by higher temperature in the tumor site;[18] however, the tumor environment itself exhibits only a slight increase of the temperature, which is most likely insufficient to trigger a quick-release of the chemical drug. *In vivo*, the heating of the tumor site has previously been realized by using temperature controlled water sacks, radio-frequency oscillators or miniature annular-phased array microwave applicators.[18] Currently, inducing hyperthermia in the narrow window (42 °C $\leq T \leq$ 43 °C) that provides optimal blood perfusion and permeability without causing severe vascular damage is difficult in clinical settings, and non-specific heating of surrounding healthy tissues may increase non-specific drug delivery, thereby inducing undesired toxicity. Therefore, a local heating instrument with a deep penetration was necessary for the TL investigation because most tumors are deeply located in organs of the human body.

In addition, the heating should be a mild, non-invasive and non-irritative operation. Recently, photothermal hyperthermia in tumors generated by plasmonic nanoparticles upon irradiation of light with wavelength in visible or near-infrared (NIR) regions has been reported.[19,20] Specifically, one of the major current interests is the application of NIR light-responsive nanomaterials. NIR light in the 650–900 nm range can penetrate tissues up to 10 cm without injuring healthy tissues due to the minimal absorption of blood and water and minimal scattering in tissues.[21] The light-responsive nanomaterials can strongly absorb NIR light and convert it into cytotoxic heat to ablate the hyperthermia-sensitive tumor cells while maintaining minimal damage to the surrounding healthy cells. Therefore, gold-based nanomaterials have recently attracted attention as a promising material for their photothermal responsive properties, good biocompatibility and low toxicity.[20] In addition, researchers have reported that the uptake capacity of spherical GNPs by tumor cells is much greater than that of rod-shaped GNPs.[22] In other words, GNP spheres accumulated specifically in tumor tissue due to a more amplified EPR effect.[23]

Among the different shapes of gold nanostructures, solid gold nanoparticles (GNPs) have been researched as the photothermal agent because of their interesting shape- and size-dependent physical and chemical properties. Due to their surface plasmon resonance (SPR), GNPs can strongly absorb light and convert this light energy to heat.[24] Although GNPs have been widely researched in the field of biomedicine, their relatively short absorption wavelength in the visible region (*ca.* 520 nm) is a major limitation for photothermal therapy. Meanwhile, hollow gold nanoparticles (HGNPs), gold nanoparticles with a spherical cavity,[25] have higher photothermal conversion ability and a more tunable (550–950 nm) absorption wavelength than GNPs due to their large cross-section.[25] Additionally, HGNPs of diameter *ca.* 50 nm have a higher rate for cancer cell internalization than GNPs, which are usually smaller than 30 nm.[26] However, the clinical applications of HGNPs for tumor therapy are limited by the following shortcomings: (1) the HGNPs aggregate quickly under physiological conditions, which is not suitable for *in vivo* drug delivery;[27] (2) the HGNP-based system may suffer from drug leakage because of their intrinsic hollow interiors and pores, subsequently causing adverse side effects;[28,29] (3) as an alternative to radical surgery, applying HGNPs alone is not sufficient for tumor therapy. From the literature, the most promising application of hyperthermia lies in its ability to act as an adjunctive therapy with the radiotherapy or chemotherapy.[30] Therefore, the combination of photothermal therapy and chemotherapy to achieve specific drug release in the tumor site is an important objective in this field.

Gold nanoparticle containing TLs can be thermally triggered to generate hyperthermia, which destroys the lipid membrane and releases the active agents. The co-delivery of DOX and HGNPs based on thermosensitive liposomal carriers (HGNPs&DOX-TLs) has recently attracted great attention for their synergistic applications involving both diagnostic and therapeutic functions in the same delivery system.[31] The thermosensitive liposome system increases the stability of the HGNPs and the loading efficiency of DOX in the blood circulation during delivery while also achieving the heat responsive drug release, which improve its anti-tumor efficiency; however, there are few reported HGNPs&DOX-TL co-delivery systems. This is an innovative study to compare the combined effect of hollow gold or solid gold inside liposomes with chemotherapeutic agents and to find how to achieve a better synergistic effect of hyperthermia and chemotherapy.

In this study, the GNPs or HGNPs, which act as a nanoswitch for killing tumor cells directly by NIR-induced hyperthermia and triggering DOX release from TLs, have been designed as a novel carrier system for combination therapy consisting of hyperthermia and a chemotherapeutic drug to treat cancer (as shown in Scheme 1). We then evaluated the NIR-triggered drug release, cytotoxicity, and *in vivo* tumor targeting using a non-invasive live animal imaging technology. Finally, the antitumor

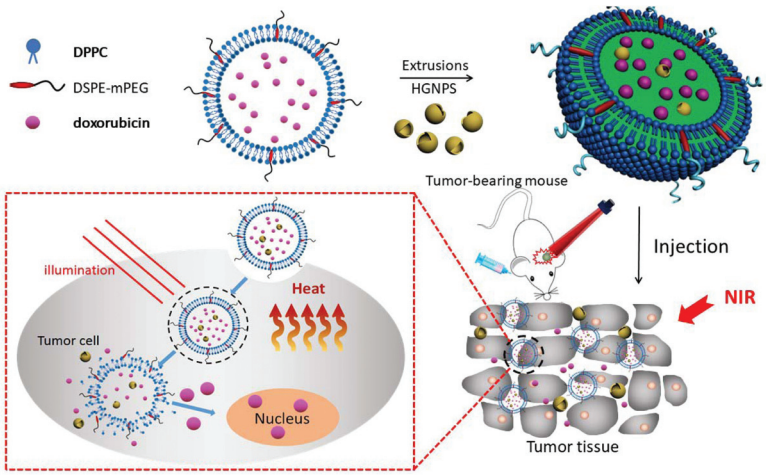

Scheme 1 The structure of HGNPs&DOX-TLs and the behaviors of entering tumor tissue and tumor cells.

efficacy of the liposome formulations was evaluated with and without NIR illumination by measuring the changes in the tumor volume in tumor bearing mice. In addition, the comparative effects of GNPs and HGNPs for thermotherapy are unknown. In this work, we aim to compare the biological and physicochemical properties of GNPs and HGNPs which were incorporated into DOX-loaded TLs for breast tumor delivery. Factors such as photothermal transformation ability, NIR-triggered drug release, cytotoxicity, intracellular uptake, *in vivo* anti-tumor efficiency, and survival period in a breast tumor model are explored.

2. Materials and methods

2.1 Materials

1,2-Dipalmitoyl-*sn-glycero*-3-phosphocholine (DPPC) and 1,2-distearoyl-*sn-glycero*-3-phosphoethanolamine-*N*-[methoxy (polyethylene glycol)-2000] (DSPE-PEG2000) were purchased from Avanti Polar Lipids Inc. (Shanghai, China). Doxorubicin (DOX) was obtained from Huafeng United Technology (Beijing, China). MTT (3-(4,5-dimethyl-thiazol-2-yl)-2,5-diphenyl-tetrazolium bromide) was purchased from Shanghai Institute of Cell Research (Shanghai, China). 1,1′-Dioctadecyl-3,3,3′,3′-tetramethyl indotricarbocyanine Iodide(Dir) was obtained from Sigma Chemical Co, Ltd (Saint Louis, MO). All the reagents were of analytical grade and used without further purification. The human fibroblast cell line (HDF) and MCF-7 cells were purchased from the NanJing KeyGen Biotech Company. All animal experiments were conducted in full compliance with the National Institute of Health Guide for the Care and Use of Laboratory Animals and approved by the Animal Ethics Committee of China Pharmaceutical University.

2.2 Preparation of solid gold nanoparticles (GNPs)

In a 100 mL round-bottomed flask, 50 mL of 250 μM $HAuCl_4$ was heated to boiling with vigorous stirring. Next, 1 mL of 1 wt% sodium citrate was added quickly, which resulted in a color change from blue to burgundy. After further stirring at the same temperature for 15 min, the resulting GNP solution was cooled to room temperature.

2.3 Preparation of hollow gold nanoparticles (HGNPs)

The preparation of hollow gold nanoparticles (HGNPs) is presented in the ESI.†

2.4. Characterization of GNPs and HGNPs based on Ag and Co templates

The morphology and size of the synthesized GNPs and HGNPs based on Ag and Co templates were both characterized by transmission electron microscopy (TEM, HT7700, Japan) with a CCD camera operating at an accelerating voltage of 100 kV. The particle size distribution of GNPs and HGNPs based on Ag and Co templates was determined by dynamic light scattering (DLS) on a Zetasizer Nano-ZS90 (Malvern Instruments, UK). The absorption spectra of GNPs and HGNPs based on Ag and Co templates ranging from 400 to 900 nm were obtained using a UV-vis spectrophotometer (Agilent 8453, USA) at 25 °C.

2.5 The preparation of DOX and HGNP loaded thermosensitive liposomes (DOX&HGNPs-TLs)

The GNPs and HGNPs were prepared according to methods 2.2 and method 2.3. The prepared HGNPs (50 mL) or GNPs (50 mL) were centrifuged for 15 min at 10 000 rpm. After discarding the supernatant, the precipitate was re-dispersed to 5 mL with citrate buffer solution (pH = 4.0).

The thermosensitive phospholipid DPPC with a phase transition temperature of 41 °C was selected to composite thermosensitive liposomes (TLs), while the phase transition temperature of the regular lipid was up to 60 °C. Meanwhile, the regular lipid such as SPC was selected to prepare plain liposomes for comparisons.

The blank TLs were first prepared by thin film methods.[32] Briefly, 30 mg DPPC and 6 mg DSPE-PEG2000 were solubilized

in chloroform and then were placed on a rotary evaporator to remove the organic solvent under reduced pressure (0.1 MPa), a lipid film on the wall of the flask was obtained. The lipid film was then hydrated with 5 mL of the above HGNP solution to prepare HGNP loaded TLs (HGNPs-TLs) *via* sonication (100 W, 10 min) at room temperature. Then sequential extrusions were executed through 800, 450, and 220 nm polycarbonate filters (11 times each) at room temperature. The sonication and extrusion processes were used to achieve higher loading efficiency of the HGNPs with a uniform size. Next, the DOX was encapsulated inside the HGNPs-TLs by the pH gradient method.[33] The outside pH of the HGNP-TL solution was titrated to pH 7.0 using 0.5 M sodium carbonate. As a result, a pH gradient was generated across the lipid bilayer. DOX was then added to the liposome solution at a 1 : 20 DOX/lipid weight ratio and mixed at 60 °C for 15 min. Finally, the amount of encapsulated DOX was removed by dialysis (14 kDa) against 0.9% NaCl (the dialysate was exchanged every 6 h for 4 times). The DOX and GNP loaded TLs (DOX&GNPs-TLs) were prepared using the same method as described above. Both The DOX loaded plain liposomes (DOX-Ls) and the DOX&HGNP loaded plain liposomes (DOX&HGNP-Ls) were prepared by the same methods with a composition of 30 mg SPC and 6 mg cholesterol.

2.6 Photothermal transformation ability of HGNPs and HGNPs-TLs

To verify the photothermal transduction ability of HGNPs, GNPs, HGNPs-TLs, GNPs-TLs, and TLs, 1 mL of these samples (Au: 75 μM) in a glass vial was irradiated by using an 808 nm NIR laser with an intensity of 3 w cm^{-2} for 10 min, and the temperature change was measured by using a digital thermometer. Both the PBS solution and blank TLs were used as the negative control. In order to compare and optimize the Au concentration for the photothermal effects, different Au concentrations (75 μM, 225 μM and 375 μM) were applied for NIR irradiation. The temperature change curves were recorded according to the procedure described above. All experiments were performed in triplicate. The photothermal imaging was carried out by monitoring the HGNP, GNP, PBS, HGNP-TL, GNP-TL and TL solutions irradiated using an 808 nm NIR laser at 1 min, 3 min, 5 min and 10 min using an infrared thermal imager (Germany, PCE-TC 3).

2.7 Characteristics of GNPs, HGNPs, DOX&HGNPs-TLs, DOX&GNPs-TLs

The particle size of HGNPs and DOX&HGNPs-TLs was measured using a Malvern Zetasizer Nano-ZS90 (Malvern instruments, UK). The particle morphology was observed by transmission electron microscopy (TEM, H-600, Hitachi, Japan). The final DOX concentration after dialysis was determined by lysing of the liposomal nanocarriers with 5% Triton X-100 and the measurement of the fluorescence value. The Au element content of the HGNPs-TLs, DOX&HGNPs-TLs and DOX&GNPs-TLs was measured using an atomic absorption spectrophotometer (AAS, Thermo Scientific ICE-3300, USA). The samples were digested with freshly prepared aqua regia (HCl/HNO_3 = 3/1, v/v) for 1 day and then diluted in deionized water for analysis.

2.8 *In vitro* temperature-triggered and NIR-triggered release of Doxorubicin

DOX release was measured at different temperatures and with or without NIR irradiation. To monitor the release of DOX, 2 mL of free DOX solution, DOX&HGNPs-TLs and DOX&GNPs-TLs were placed in separated dialysis bags (14KD) and immersed in 20 mL of release medium (0.9% NaCl) at 37 °C and 42.5 °C in a water bath (100 rpm, water bath, China Taicang Huamei instrument), respectively. Samples (2 mL) from the release medium were taken at predetermined time intervals for 24 h. The concentration of DOX was determined according to the method in 2.6. Also, in order to evaluate the feasibility of triggering DOX release under NIR illumination, the DOX release by 808 nm NIR irradiation was carried out at 3 W cm^{-2} and the beam spot size of 20 mm for 30 min. Then, at 10 min, 20 min and 30 min, the DOX-TLs, DOX&HGNPs-TLs and DOX&GNPs-TLs were centrifuged at 3000 rpm for 5 min, and the concentration of the released DOX in the supernatant before and after laser irradiation was determined by the fluorescence method.

2.9 *In vitro* biological evaluation

2.9.1 Cell culture. The human fibroblast cell line (HDF) was cultured in cell plates using DMEM medium with 10% fetal bovine serum (FBS) at 37 °C under a 5% CO_2 atmosphere. Human breast cancer cells (MCF-7 cells) were cultured in cell plates using 1640 medium with 10% fetal bovine serum (FBS) at 37 °C under a 5% CO_2 atmosphere.

2.9.2 The comparative cytotoxicity study of HGNPs prepared by the silver and cobalt template-engaged replacement reaction method on HDF cells. The cytotoxicity of HGNPs on the human fibroblast cells was evaluated using the 3-(4,5-dimethylthiazol-2-yl)-2,5-diphenyltetrazolium bromide (MTT) colorimetric test by calculating the cell viability percentage (%). The HDF cells were seeded in a 96-well plate at a density of 5000 cells per well. After 24 h of incubation, the HDF cells were treated with increasing concentrations of HGNPs. Then MTT was added and incubated for 4 h at 37 °C to form formazan crystals. The medium was removed before 150 μl of dimethyl sulfoxide (DMSO) was added to each well and the absorbance of dissolved formazan was measured at 570 nm using a Microplate Reader (BioTek USA). The cell viability was calculated by the following formulation:

$$\text{cell viability } (\%) = \frac{OD_{sample} - OD_{blank}}{OD_{control} - OD_{blank}} \times 100\%$$

where the OD_{sample} is the absorbance of cells incubated with the nanoparticle sample; the OD_{blank} is the absorbance of the blank PSB without cells and the $OD_{control}$ is the absorbance of the blank medium with cells. The toxicity of the samples was expressed as the inhibitory concentration at which 50% of cell growth inhibition was obtained (IC_{50}).

2.9.3 The efficiency of liposome chemotherapy combined with photothermal therapy on MCF-7 cells. MCF-7 cells were seeded identically on 96-well plates as stated previously. The cells were incubated with free DOX solution, DOX&HGNPs-TLs, DOX&GNPs-TLs, HGNPs-TLs, DOX-TLs and DOX-Ls at DOX each at concentrations of 1.0, 3.0, and 5.0 μg mL^{-1} for 6 h, and followed by applying an 808 nm laser at 2.0 W cm^{-2} for 10 min every hour for the first 6 h. After an additional 18 h of incubation (30 h total), the drug was removed and replaced with 100 μL of fresh media mixed with 10 μL MTT. After 4 h of MTT incubation, 100 μL of media was removed and 150 μL of dimethyl sulfoxide (DMSO) was added to solubilize the formazan. A microplate reader (Bio Tek Instruments, Inc.) was used to read the absorbance at 540 nm. The cytotoxicity of these formulations on the MCF-7 was calculated, respectively, according to the equation above.

2.9.4 Intracellular uptake assay. Prior to the evaluation of *in vivo* therapeutic efficacy of the co-delivery system, the *in vitro* cellular uptake of DOX and HGNPs was investigated. The MCF-7 cells were cultured in 6-well plates at 4 × 105 cells per well and once grown to *ca.* 80% confluence, the cells were given free DOX solution, DOX&HGNPs-L and DOX&HGNPs-TL at DOX concentrations of 3.0 μg mL^{-1} and then incubated for 2, 4 and 6 h, respectively. Later, the medium was removed and the cells were washed 3 times with PBS buffer to remove any excessive or unbound drugs or nanoparticles in the plate. The cells were then stained by using DAPI for 15 min, fixed by using 4% of paraformaldehyde, and subsequently washed twice with PBS. Finally, the MCF-7 cells were observed under an inverted fluorescence microscope (DSZ2000, China).

The TEM thin section was used to visualize the interactions of HGNPs-TLs with MCF-7 cells. For this, the cells that were exposed to DOX&HGNPs-L and DOX&HGNPs-TL at a DOX dose of 3 μg mL^{-1} for 24 hours were fixed with 2.5% glutaraldehyde in 0.1 M sodium cacodylate buffer at a pH of 7.2. Then, the inserts were post-fixed with 1.0% osmium tetroxide and rinsed with buffer at a pH of 7.2 after 2 h. Next, inserts with cells were dehydrated with 30%, 70%, 85%, and 95% ethanol, each for 10–15 min and finally with 100% ethanol for 1 h. After dehydration, the cells were then infiltrated with 1 : 1 Spurrs/Quetol resin to 100% ethanol overnight followed by 100% Spurrs/Quetol resin overnight on a mixing turntable. Finally, the inserts were embedded in fresh Spurrs/Quetol resin and were ready for sectioning. For ultrathin sections, samples were cut to about 50 nm and mounted on copper grids. Sections were stained with lead citrate and uranyl acetate and observed with a TEM (H-600, Hitachi, Japan).

2.10 *In vivo* evaluation

2.10.1 Animals and tumor implantation. Animal protocols were performed under the guidelines for humans and the responsible use of animals in research set by China Pharmaceutical University. Female nude mice (20 ± 2 g) about 3–4 weeks old were purchased from Qinglongshan Farms (Nanjing, China). The animals were provided with *ad libitum* access to food and water and maintained at 25 °C with a relative humidity of 55%. About 2 × 106 MCF-7 cells were subcutaneously injected into the right forelimb armpit of the nude mice. The tumor size was measured and the tumor volume was calculated as $V = AB^2/2$, where A and B are the maximum and minimum diameters of a tumor, respectively.

2.10.2 *In vivo* targeting evaluation and photothermal transformation ability evaluation. When the tumor size reached 200 mm^3, the tumor-bearing mice were randomly divided into three groups (n = 6), and were injected intravenously (IV) with free Dir, Dir&HGNPs-L or Dir&HGNPs-TLs with an equivalent dose of 2 mg kg^{-1} Dir, respectively. The imaging experiments were performed at 1 h, 2 h, 4 h, and 8 h after injection. After 8 h, the mice were sacrificed and the main organs including heart, liver, spleen, lung, kidney, brain and the tumor were harvested. The fluorescence intensity was determined by using a Kodakin *in vivo* imaging system FX PRO (Kodak, USA) equipped with an excitation band pass filter at 720 nm and an emission at 790 nm.

Photothermal transformation ability evaluation was carried out similarly. When the tumor size reached 200 mm^3, the tumor-bearing mice were randomly divided into three groups including the TL group, the HGNPs-TL group and the GNPs-TL group. The temperature changes at the tumor sites were monitored using a thermal imaging camera at the 8 h after the IV administration.

2.10.3 Antitumor activity *in vivo*. When the tumor volume reached 100–150 mm^3, the mice were randomly divided into eight groups (n = 5). The groups are defined as follows: (A) saline, (B) saline + Laser, (C) DOX solution, (D) DOX-TL, (E) HGNPs-TL + NIR, (F) DOX&GNPs-TL + NIR, and (G) DOX&HGNPs-TL + NIR. The samples (200 μL) at the DOX concentration of 0.15 mg mL^{-1} and Au concentration of 6.15 ng mL^{-1} were IV injections *via* a tail vein at three-day intervals for four times, respectively (Scheme 2). For the groups with laser irradiation, the mice were subjected to 808 nm laser irradiation (2 W cm^{-2}, 5 min) 24 h after IV administration (Scheme 2). The tumor length and width were measured using a caliper every two days. The animals were sacrificed on the 30th day and the tumors were excised, weighed, and photographed. The body weight was measured simultaneously and was taken as a parameter of systemic toxicity.

2.11 Histology analysis

On the 30th day, all experimental mice were sacrificed after treatment. The five main organs (heart, liver, spleen, lung and kidney) were excised, fixed with 4% paraformaldehyde, and embedded in paraffin blocks for hematoxylin and eosin (H&E) staining. After H&E staining, the sections were observed and photographed using an optical microscope (magnification: 10 × 10).

2.12 Data analysis

All analysis data are given as means ± SD. The results were analyzed by the Student's t-test (SPSS 17.0, China). $*p < 0.05$ was considered significant. $**p < 0.01$,$***p < 0.001$ and $\#p < 0.0001$ were highly significant compared to the corresponding control.

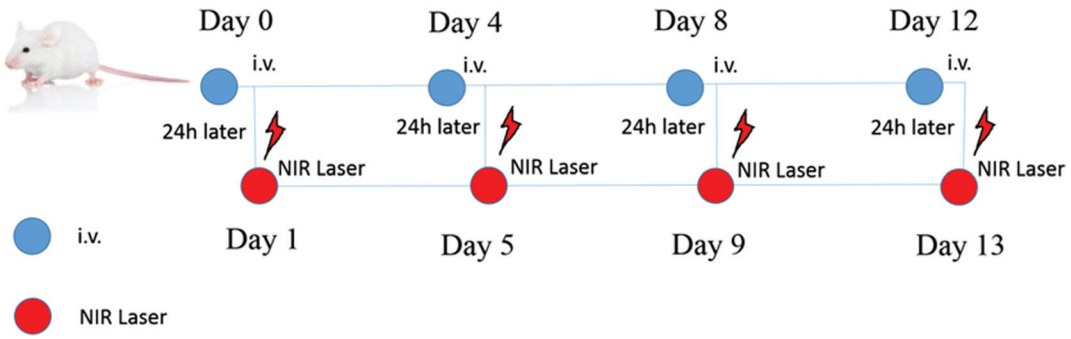

Scheme 2 The administration and laser irradiation schedule of the liposomes for the mice (n = 5).

3. Results and discussion

3.1 GNP and HGNP characterization

The characteristics of GNPs and HGNPs are shown in Fig. 1. The size of GNPs was 23.2 nm with the PDI of 0.392 which is noticeably smaller than that of the HGNPs (Fig. 1A–C). According to Fig. 1D–F, TEM images revealed that the morphology of the typical HGNP is spherical and hollow, although some have irregular shapes or incomplete shells prepared by Ag template methods. The size diameter of HGNPs by Ag template methods was 50.3 nm with a PI of 0.23. The shell thickness was 6 nm. The synthesized HGNPs by Co template methods were more uniform, around 60.7 nm, with a PI of 0.20 and complete shell thickness of 5 nm (Fig. 1G–I). The HGNPs prepared as discussed above all had an effective absorption peak around 800 nm for maximum light penetration into tissue. Moreover, the prepared HGNPs (Co) showed superior safety to the HGNPs (Ag) because the cell viability decreased to 10% with HGNPs (Ag) while the cell viability remained above 90% for HGNPs (Co) at the same high concentration of 200 μM (Fig. S1†). The substantial cell inhibition of HGNPs (Ag) could be due to the absorption of Ag^{+} on the surface of the HGNPs, which caused continued toxicity towards the HDF cells.[34] Therefore, the HGNPs (Co) were taken for the next studies. The synthesized GNPs and HGNPs are quite stable because of electrostatic repulsion caused by the adsorption of citrate ions, resulting in an overall negative charge on them. However, to improve their stability against aggregation in physiological buffers and other high-ionic strength solutions, the HGNPs are further stabilized sterically by PVP and the effect of PVP on the formulation of HGNPs will be further studied.

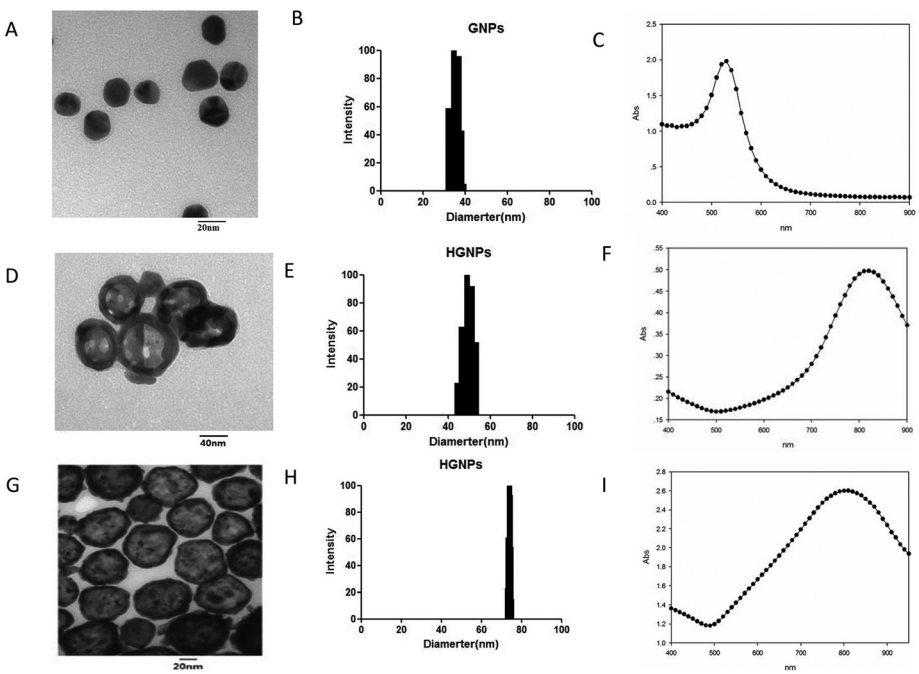

Fig. 1 Size distribution (A), the morphology (B) and the absorption spectra (C) of gold nanoparticles. Size distribution (D), the morphology (E) and the absorption spectra (F) of hollow gold nanoparticles by the Ag template method. Size distribution (G), the morphology (H) and the absorption spectra(I) of hollow gold nanoparticles by the Co template method.

3.2 The effect of PVP on the formulation of HGNPs by Co template methods

Although HGNPs possess a relatively low thermal mass that allows them to dissipate the heat to the local cancer environment efficiently, the synthesis of HGNPs is challenging in terms of reproducibility, especially those with SPRs in the desired NIR (*e.g.* 800 nm) region, and therefore, the polymer poly(vinylpyrrolidone) (PVP K30) was utilized as an efficient stabilizing agent for the synthesis according to the reports that PVP with higher molecular weights such as K90 and longer chains promotes bridging flocculation of the small particles due to loops, tails and trains extending to the solution from the particle surface resulting in large flocculation. The PVP K15 chain was too small to provide sufficient steric stabilization to smaller particles in the long term.[35] In contrast, PVP K30 provides sufficient steric stabilization to HGNPs, and was therefore selected as the best choice for this study. As shown in Fig. (2c), the average SPR absorption peak of the HGNPs synthesized with PVP was 800 nm and the non-PVP stabilized HGNPs yielded an average SPR absorption peak of 650 nm, indicating that those prepared with PVP are significantly red-shifted (peak at approximately 800 nm *vs.* 650 nm). When PVP was used, there is significant broadening of the SPR absorption. The morphology of HGNPs synthesized without PVP exhibited thick gold shells and large size heterogeneity, as shown in Fig. (2a). In contrast, HGNPs synthesized with PVP possessed thin gold shells and uniform size distribution (Fig. 2b), which is essential for the desired SPR absorption maximum. This is explained by two reasons: (1) PVP could stabilize larger cobalt particles to form with low concentrations of sodium citrate, while without PVP, flocculation often recurs, and (2) PVP could kinetically control the formation of the gold shell, which is normally a fast process, by forming a dense shell on the surface of the cobalt particles resulting in slowing the gold reduction and making thinner (and thus more red-shifted) shells possible (Fig. 3). Moreover, the addition of PVP increased the stability of the HGNPs for 24 h without a significant change of PDI and size diameter, which would inhibit the flocculation in the systemic circulation (Fig. S2†). This highly reproducible synthesis method with absorbing HGNPs using PVP as a template stabilizing agent was used in the next studies.

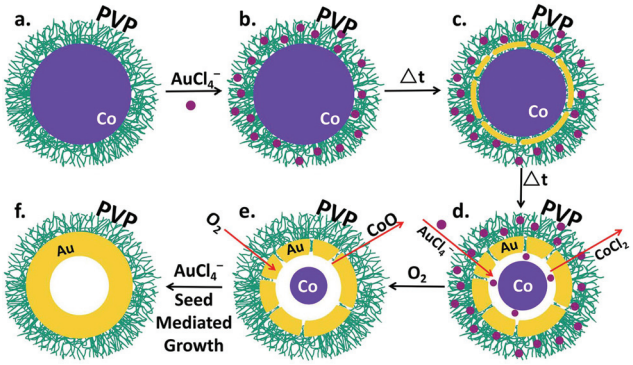

Fig. 3 . The mechanism for the effect of PVP on the preparation of HGNPs. (a) (Please use either all capital letters or all lower cases for figure sections) Attachment of PVP on the Co nanoparticles surface; (b) interaction of $AuCl_4^-$ with Co nanoparticles; (c) reduction of Au^{3+} by Co^0($3Co + 2AuCl_4^- = 2Au + 3Co^{2+} + 8Cl^-$); (d) initialization of the gold shell formation; (e) oxidation of remaining Co nanoparticles; and (f) formation of hollow gold nanoparticles with the presence of PVP.

3.3 The effect of concentration of H $AuCl_4$ on the formulation of HGNPs

The morphologies of HGNPs with the addition of different volumes of $HAuCl_4$ are shown in Fig. 4(A–D). The results showed that the HGNPs were spherical and uniform when the volume of $HAuCl_4$ was 200 μL and 300 μL. When the volume of the $HAuCl_4$ was increased to 400 μL, some irregular gold nanoparticles appeared (as the black arrow indicates in Fig. 4C) and the shapes of the HGNPs turn into solid-particle-like when the volume of $HAuCl_4$ reached 500 μL. As shown in Fig. 4E, the average SPR absorption peak of the HGNPs synthesized with 200 μL, 300 μL, 400 μL and 500 μL of $HAuCl_4$ was at 850 nm, 800 nm, 700 nm and 650 nm, respectively, which indicated that the SPR position of the HGNP can be tuned to cover the entire visible to NIR region by changing the shape and shell thickness (Fig. 4E). It was concluded that increasing the gold wall thickness at a constant particle size will increase as the volume of the $HAuCl_4$ increases (Fig. 4F), which results in the blue-shift of the absorption band. The band shifts to higher energy because HGNPs take on more solid-particle-like properties when their inner diameter decreases. Because solid gold particles at these sizes have plasmon bands at approximately 520 nm, the absorption will always shift in this direction as the

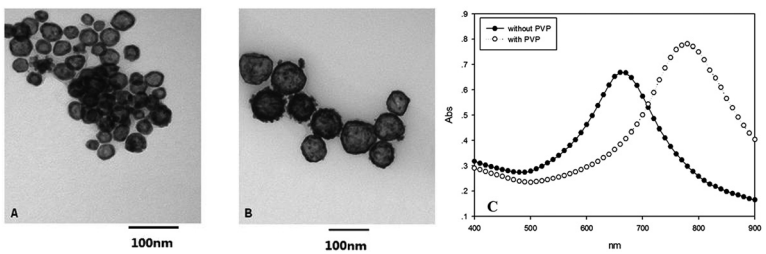

Fig. 2 The morphology of preparation without or with PVP (A is prepared without PVP; B is prepared with PVP) by TEM. C is the absorption spectra of HGNPs preparation without or with PVP.

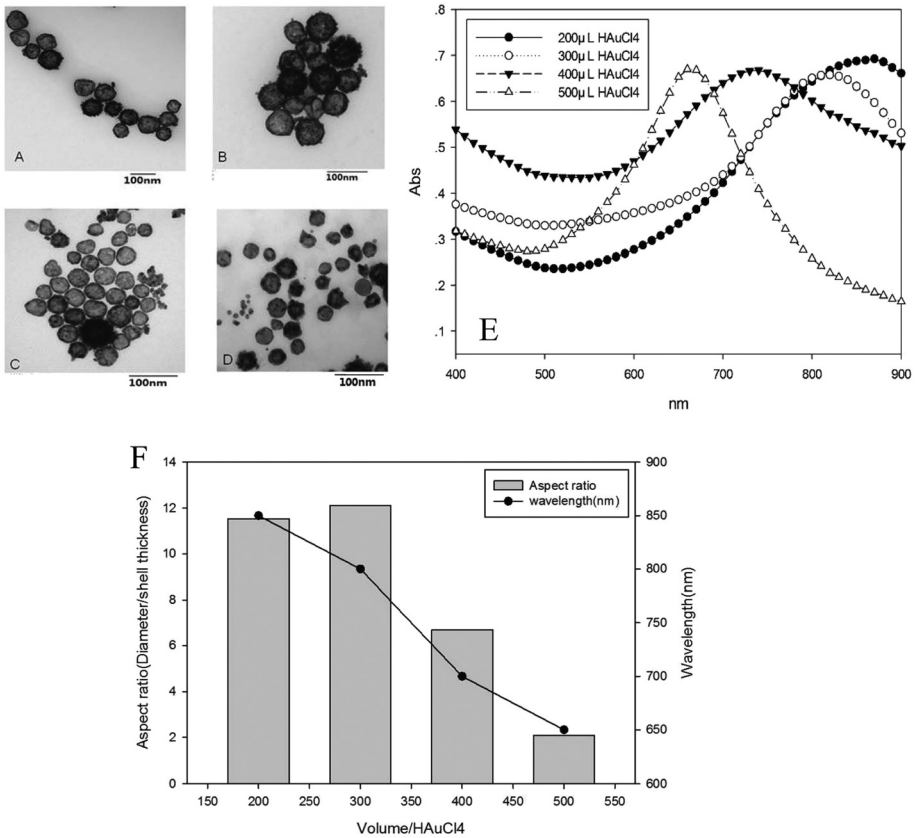

Fig. 4 The morphology of HGNPs by TEM (A: 200 μL; B: 300 μL; C: 400 μL; D: 500 μL). E is the absorption spectra of hollow gold nanoparticles prepared with different doses of $HAuCl_4$. F. The changes of the aspect ratio (size diameter/shell thickness) and the absorption peak with different doses of $HAuCl_4$.

wall thickness increases. This is predicted by previous work[36] that the plasmon absorbance maximum wavelength (λ_{max}) will linearly increase with the increased ratio of the particle size and wall thickness, which is correlated with our results.

In this study, since the excitation wavelength of the laser is 808 nm, 300 μL of $HAuCl_4$ was chosen in the next synthetic procedure to achieve the best photothermal transduction ability.

3.4 DOX&GNPs-TL and DOX&HGNPs-TL characterization

The prepared DOX&HGNPs-TLs exhibited a size of 196.8 ± 3.2 nm with a poly-dispersity index (PDI) of less than 0.2. According to the TEM images, most of the HGNPs or GNPs were either associated with the surface of liposomes or encapsulated inside the hydrophilic core of liposomes (Fig. 5). In addition, the prepared DOX&HGNPs-TL and DOX&GNPs-TL possessed a negative zeta potential of −29.55 ± 2.45 mV and −28.75 ± 3.79 mV. The DOX&HGNPs-TLs were stable for at least 30 days without any significant changes in the hydrodynamic diameter when stored at 4 °C (Table S1†) which indicated that the liposome increased the stability of HGNPs effectively. The encapsulation efficiency of DOX in the liposome was (89.3 ± 1.37)% which is a little lower compared with the reported results using the same method.[37] The reason may be the occupation of the hydrophilic core by the HGNPs.

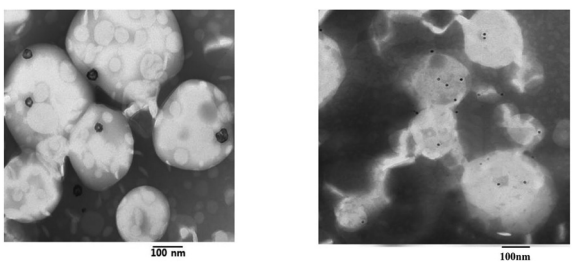

Fig. 5 The morphology of HGNPs-TLs (A) and GNPs-TLs (B).

Moreover, the encapsulation efficiency of HGNPs was determined as (10.87 ± 0.46)% in the liposomes and that of the GNPs was determined as (21.27 ± 1.38)% in the liposomes. Using the same preparation method, more GNPs were loaded inside the liposomes which may be due to the smaller size of the GNPs. Above all, the DOX and the HGNPs were loaded inside the TL effectively for further experiments.

3.5 The comparison of photothermal transformation ability of HGNPs-TLs and GNPs-TLs

In order to assess the light-to-heat conversion of HGNPs and HGNPs-TLs compared to GNPs and GNPs-TLs for photothermal ablation of tumors, we measured the temperature changes

of formulation for 10 min under NIR illumination. With the absorption of NIR, the HGNPs could exhibit photothermal transformation ability, which makes the temperature in the cancer area rise rapidly and thus induce the quick release of DOX by the thermosensitive liposomes to kill the cancer cells combined with the hyperthermia. As shown in Fig. 6, there was a steep temperature increase over the first 2 minutes for HGNPs and HGNPs-TLs, and the temperature reached above 40 °C in 2 minutes for HGNPs while the GNPs needed 4 minutes to reach the same temperature. This suggests that the HGNPs exhibited stronger photothermal transformation ability than GNPs (Fig. 6A). The results can be explained by the large cross-section of absorption attributed to the cavity structure of HGNPs.[38] An obvious concentration-dependent temperature increase was observed. As shown in Fig. 6C, 45 °C could be achieved within 5 min at relatively low concentration levels (75 μM). Although the greater photothermal conversion effect was obtained by higher HGNP concentration, further cytotoxicity and other influential factors should also be taken into consideration to select a reasonable HGNP concentration. Additionally, there was less temperature change (37 °C for 10 min) in the GNPs, possibly due to the relatively short absorption wavelength (*ca.* 520 nm). Moreover, there was a continued temperature increase of HGNPs-TLs during the 10 min (ΔT of *ca.* 21 °C) of laser illumination which showed a significant difference with the GNPs-TL (ΔT of *ca.* 13.3 °C), TL (ΔT of 3 °C) and PBS (ΔT of *ca.* 1.5 °C), indicating that encapsulation into the liposomes will not affect the photothermal transduction efficiency of HGNPs (Fig. 6B). Based on the above results, this *in vitro* study validates that the HGNPs-TLs could facilitate hyperthermia in a short time period to achieve the thermotheraputic effect, and mild hyperthermia could generally ablate tumor tissue globally or locally at 39–42 °C. The photothermal imaging was consistent with this conclusion (Fig. 6C).

3.6 Temperature-triggered and NIR triggered DOX release behavior from liposomes

The doxorubicin loading and release properties of doxorubicin-loaded DOX&HGNPs-TLs and DOX&GNPs-TLs under various conditions were evaluated.

The cumulative release curves of DOX from free DOX solution, DOX&HGNPs-L and DOX&HGNPs-TL in PBS at 37 °C and 42 °C are shown in Fig. 7A. An initial burst release of over 80% was observed at 1 h triggered by hyperpyrexia as expected for DOX&HGNPs-TLs. The release behavior indicated that the DOX&HGNPs-TL achieved almost total drug release at 42 °C (slightly above Tm) while there was less than 10% at 37 °C. The DOX&HGNPs-L reached about 60% release at 42 °C, which is close to the release content at 37 °C. It was reported that a liposome formulation with increased release rates at regional hyperthermic temperatures is particularly advantageous in delivering drugs to a heterogeneously heated tumor. The results revealed the DOX&HGNPs-L composed of SPC induced higher leakage at 37 °C in the systemic circulation, while the DOX&HGNPs-TLs increased the rigidity of the liposomal membrane due to the presence of the DPPC, reducing the drug

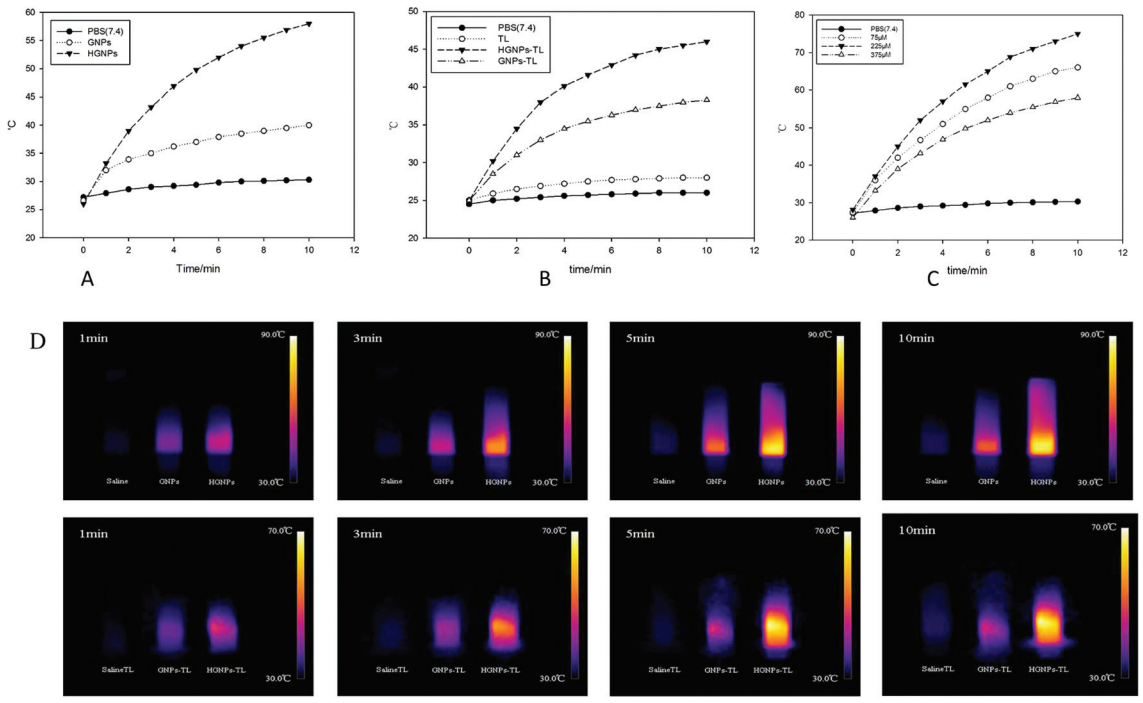

Fig. 6 A. Temperature change of HGNPs, GNPs and PBS after NIR irradiation for 10 minutes. B. Temperature change of HGNPs-TLs, GNPs-TLs, TLs and PBS after NIR irradiation for 10 minutes. C. Temperature change of different concentration (75 μM, 225 μM and 375 μM) hollow gold nanoparticles after NIR irradiation for 10 minutes. D. Photothermal imaging was carried out by monitoring the HGNP, GNP, PBS, HGNP-TL, GNP-TL and TL solutions irradiated using an 808 nm NIR laser.

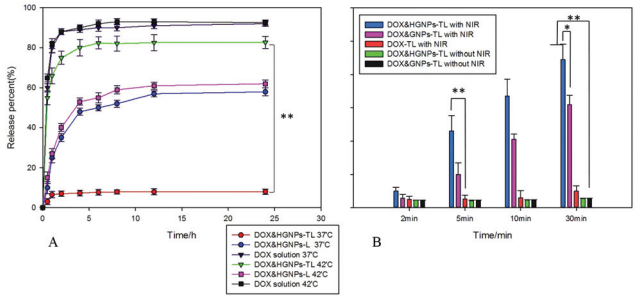

Fig. 7 DOX release from DOX solution, DOX&HGNPs-TL and DOX&HGNPs-L at 37 °C and 42 °C (A). B. Percentage of released DOX from liposomes with HGNPs, GNPs and the control, which were treated and untreated with continued laser (power density ~12 mW cm^{-2}). Schematic diagram of the DOX release from DOX&HGNPs-TLs under NIR-laser irradiation.

leakage at 37 °C and lessening the side effect for the normal tissue. The characteristics of temperature-triggered release for DOX&HGNPs-TLs could effectively improve the targeting property of DOX in tumor therapy (Scheme 3).

Then, we explored the release profile of DOX from liposomes under the laser irradiation. As shown in Fig. 7B, liposomes with HGNPs released more than 60% of DOX within 10 min, while 40% release was shown in the DOX&GNP-TL group due to the relatively short absorption wavelength (*ca.* 520 nm) of GNPs and less than 10% percentage release was observed in the DOX-TL group. Moreover, the DOX release in the DOX&HGNP-TL group and the DOX&GNP-TL group significantly increased with the increase of laser exposure time. The DOX release was boosted to 83% after 30 min NIR irradiation, but the non-irradiated group showed a small amount of DOX release in a non-triggered manner. Therefore, the DOX release from DOX&HGNPs-TLs can be controlled by the NIR laser. In conclusion, results suggest that the photothermal transduction ability of HGNPs inside TLs could increase the temperature above the phase transition temperature and trigger the release of DOX.

3.7 The cytotoxicity of DOX&HGNPs-TLs for chemo-thermotherapy

The cellular toxicity of DOX, DOX&GNPs-TLs, DOX&HGNPs-TLs, HGNPs-TLs, DOX-TLs and DOX-Ls for 48h without laser illumination was studied at 37 °C. Since the viabilities of control and HGNP-treated groups were 100% and 91%, respectively, we could confirm that there was no cytotoxicity in HGNP based formulations. Compared with the liposome formulations, 60% of the MCF-7 cells survived, when the concentration of DOX was 5 μg mL^{-1}, which indicated that the encapsulation of DOX&HGNPs into the liposomes significantly decreased its cytotoxic effect as exemplified in Fig. 8. This is possibly due to the fact that cells would have less access to DOX within the inner phase of the liposomes. Moreover, as seen from Fig. 8, the viability of plain liposomes composed of SPC also decreased to 70% with the increase of the DOX while the TL formulations did not affect the viability of the cells. The results are correlated with that of *in vitro* drug release behavior. In addition, the cytotoxicity of DOX&GNPs-TLs increased with the increase of concentration, which may be attributed to the high concentration of Au absorption on the liposomes compared with the DOX&HGNPs-TLs. With the incubation at 37 °C, the reduction of cytotoxicity by DOX&HGNPs-TLs was due to the negligible release of DOX from the liposomes.

3.8 The efficiency of liposome chemotherapy combined with photothermal therapy on MCF-7 cells

To further investigate the antitumor activity of the chemo-thermotherapeutic combination treatment with DOX&HGNPs-TLs, a total of 6 groups were tested with the MTT assay. The MCF-7 cell viabilities of all samples gradually increased as the drug concentration increased. As shown in Fig. 9, the different liposome formulations showed significant differences in cytotoxicity. The DOX&HGNPs-TLs group exhibited higher toxicity than the only NIR + HGNP treated group and the free DOX treated group due to the synergy of NIR laser triggered DOX release and the photothermal effect ($*p < 0.05$). DOX&HGNPs-TLs exhibited highest cytotoxicity with the 40% of survival viability which showed a significant difference ($p < 0.05$) with the free DOX group and the DOX&GNP-TL group, due to the photothermal transformation ability of HGNPs inside the liposome, which is stronger than that of the GNPs, triggering the DOX to release from the TLs by hyperthermia. Importantly, the DOX-TLs possessed the lowest cytotoxicity, since only slight release was triggered by the illumination in the case of liposomes without HGNPs. Above all, the combination of smart-

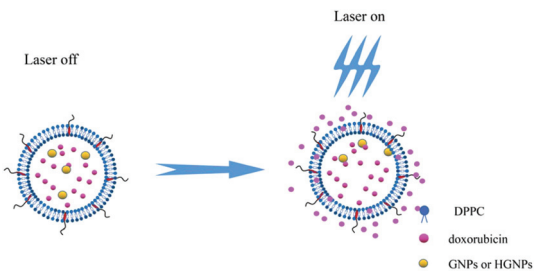

Scheme 3 The mechanism for the laser illumination on the release behavior of the DOX&HGNPs-TLs.

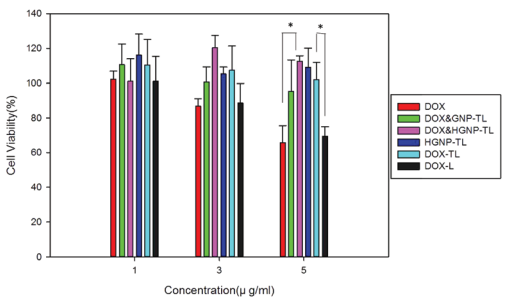

Fig. 8 Cell viability of DOX, DOX&GNPs-TLs, DOX&HGNPs-TLs, HGNPs-TLs, DOX-TLs and DOX-Ls for 48 h without NIR irradiation (n = 6, $*P < 0.05$).

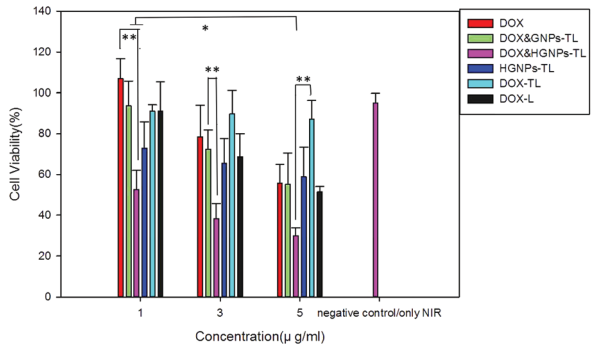

Fig. 9 Cell viability of DOX, DOX&GNPs-TLs, DOX&HGNPs-TLs, HGNPs-TLs, DOX-TLs and DOX-Ls for 48 h after NIR irradiation (n = 6, *P < 0.05, **P < 0.01).

released chemotherapy and photothermal therapy with DOX&GNPs-TLs showed significantly greater antitumor activity than any solo-treatment with HGNPs-TLs alone, free DOX or DOX-TLs *in vitro*. This enhanced antitumor effect can be attributed to both the cytotoxic effect of quickly released DOX from DOX&HGNPs-TLs and the photothermal effect mediated by HGNPs under NIR laser irradiation.

3.9 Intracellular DOX, GNP and HGNP uptake

To reveal the cellular uptake of the DOX and the liposomes inside tumor cells, the intracellular DOX was detected by using a microscope at 2 h, 4 h and 6 h, as shown in Fig. 10. DOX detected inside tumor cells increased from 2 h to 4 h for all the formulations. Furthermore, there is no significant difference in the intracellular fluorescence intensity of DOX between 4 h and 6 h, possibly due to the internal saturation of the drug. However, increased DOX was observed in the liposome groups at 6h, and therefore, the DOX&HGNPs-TLs and DOX&HGNPs-Ls displayed the highest intracellular DOX content compared to the free DOX solution at 4 h and 6 h which was presumably generated by the suitable particle size-mediated cellular uptake, the membrane stability, and fluidity of the liposome bilayer.[39] Owing to this enhanced cellular uptake, the effectively improved cytotoxicity of DOX&HGNPs-TLs with the laser irradiation is shown in Fig. 9.

In order to confirm the cellular uptake of HGNP-containing liposomes and the distribution of HGNPs inside tumor cells, MCF-7 cells were incubated with the DOX&HGNPs-TLs and

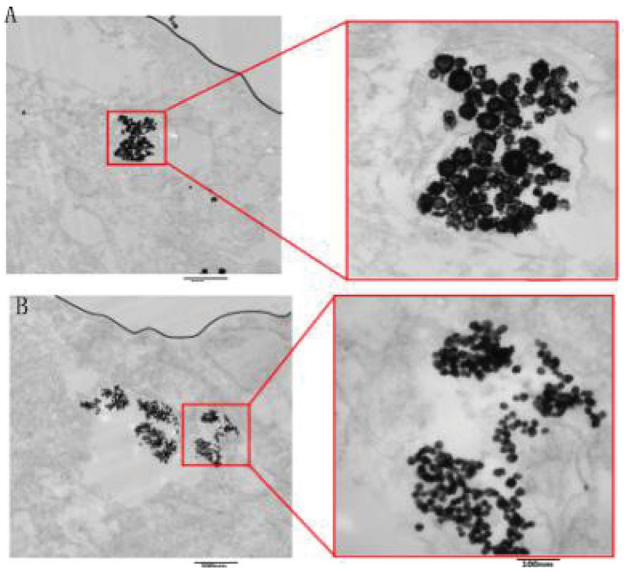

Fig. 11 TEM thin sections of the cell uptake of GNPs and HGNPs DOX&GNPs-TLs(A) and DOX&HGNPs-TLs(B) at 6 h.

DOX&GNPs-TLs for 6 h and observed by TEM (Fig. 11). As shown in the TEM images, the HGNPs and GNPs were observed in the cytoplasm of MCF-7 cells after 6 h, confirming the successful cellular uptake of HGNP- and GNP-loaded liposomes by MCF-7 cells. From the image, the uptake of GNPs was noticeably more than that of HGNPs due to the smaller size, but the photothermal transformation ability of HGNPs in cells was better than that of GNPs. This further supports the remarkable photothermal therapy for HGNPs due to their special structure.

3.10 *In vivo* targeting

In this study, the *in vivo* biodistribution of liposomes in MCF-7 tumor-bearing mice was investigated using a non-invasive NIR optical imaging technique. The tumor-bearing mice were injected with Dir, Dir&HGNPs-L and Dir&HGNPs-TLs, respectively. Fig. 12A shows the real-time images of the three formulations in the tumor-bearing mice, in which the whole bodies of live mice were monitored at 1 h, 2 h, 4 h and 8 h after administration, respectively. During the living imaging test, most of the Dir accumulated in liver 4 h after intravenous administration of the liposome formulations, most likely due

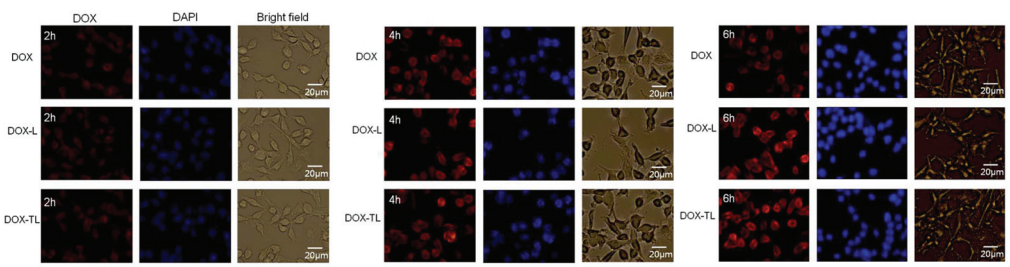

Fig. 10 Cell uptake of DOX, DOX-Ls and DOX-TLs at 2, 4 and 6 h.

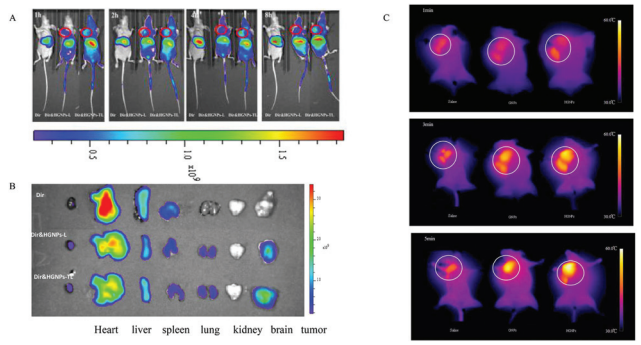

Fig. 12 (A) *In vivo* imaging of tumor-bearing mice after administration of Dir, Dir&HGNPs-L and Dir&HGNPs-TLs (B) *Ex vivo* images of tissues including heart, liver, spleen, lung, kidney, brain and tumor collected at 8 h post-injection of Dir, Dir&HGNPs-TL and Dir&HGNPs-TL. (C). IR thermal images of MCF-7 tumor-bearing mice after injection of saline, GNPs-TLs and HGNPs-TLs with laser irradiation (808 nm, 0.5 W cm) at 8 h after the administration. The white circle represents the tumor area.

to the phagocytosis of nanoparticles by macrophages and immune cells.[40] However, the preferential accumulation of fluorescence was notable in the tumor site rather than the liver or other normal tissues at 8 h after injection for Dir&HGNPs-L and Dir&HGNPs-TL groups, which provides decisive evidence that the liposomes were available for tumor-specific drug delivery. This tumor target ability of liposomes might be due to the enhanced permeability and retention (EPR) effect. Moreover, the Dir&HGNPs-TLs showed much higher tumor targeting efficiency than Dir&HGNPs-L, confirmed by the enhanced accumulation of TLs in tumors. As shown in Fig. 12B, the *ex vivo* fluorescent image of excised tumors further confirmed the higher fluorescence accumulation in the tumors of the Dir&HGNP-TL group compared with the Dir&HGNP-L group, which resulted in prolonged circulation and reduced elimination of TLs by the incorporation of PEG-DSPE. In this case, the drug clearance of the TLs would decrease, possibly due to its increased accumulation in tumor.

Thermal imaging with infrared thermal imaging apparatus was used to monitor the temperature changes in the tumor area for the liposome groups. From the images, the local tumor temperature with TLs under the same irradiation conditions showed a slight temperature elevation. In addition, the local tumor temperature increased rapidly by above 20 °C within 5 min for the HGNP-TL and GNP-TL groups under the irradiation (Fig. 12C). In comparison, the temperature for the HGNPs-TLs showed apparently a higher level than the GNPs-TLs, which supports the superior photothermal transformation ability of the HGNPs-TLs. Previous studies indicated that a temperature increase by 20 °C is sufficient to induce thermal damage to the cancer cells in the identified tissue area with irreversible tissue injury.[41] Above all, the *in vivo* result was consistent with the *in vitro* result.

3.11 Antitumor activity *in vivo*

To evaluate the antitumor efficacy of the DOX&HGNPs-TLs for combined chemo-thermotherapy, seven formulations were administered intravenously into the tumor-bearing mice (n = 5). The changes in the tumor volume, the final tumor weight and the body weight treated with test formulations are presented in Fig. 13; saline was used as the negative control.

As shown in Fig. 13A, mice of the saline + NIR group showed a similar rapid increase in the tumor size to the negative group, demonstrating that NIR itself has no cytotoxic effect. Subsequently, the phototherapy of HGNPs-TL + NIR was studied and the relative tumor size was reduced to 40%, proving the efficiency of phototherapy. This can be attributed to the rapid temperature elevation caused by the HGNPs with the illumination, resulting in the death of cancer cells. Notably, HGNPs&DOX-TLs without NIR possessed a lower inhibiting effect than other DOX formulation due to the absence of heat to trigger the release of DOX from the liposomes. At 30 days after the administration, the DOX group, DOX-TLs, HGNPs-TL + NIR and the DOX&HGNPs-TL + NIR group suppressed tumor sizes to 52.14%, 68.43%, 40%, and 18.8% com-

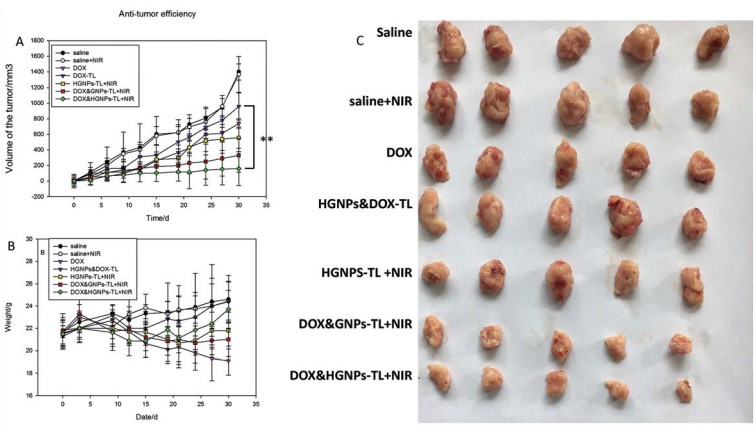

Fig. 13 *In vivo* antitumor efficacy of saline, saline &NIR, DOX, DOX-TLs, HGNPs-TLs&NIR, DOX&GNPs-TL + NIR and DOX&HGNPs-TL + NIR in tumor-bearing mouse models. (A) Tumor volume changes, (B) body weight changes during the treatment, and (C) tumor tissue weight in the last day of test (*P < 0.05,**P < 0.01).

pared with the saline group, respectively. The tumor tissues for different groups (n = 5) at 30 days are listed in Fig. 13C and are consistent with the curves of the tumor growth. The DOX&HGNP-TL + NIR group exhibited the most significant antitumor ability compared to other groups, which supports the excellent synergistic antitumor effect of chemotherapy and photothermal therapy. Although the EE of the GNPs in liposomes was higher than the HGNPS, the insufficient photothermal ability caused lower efficiency compared with the HGNP-TL. Many studies have shown that hyperthermia enhances chemotherapy *via* changes on blood flow, tumor microenvironment, signal transduction, and protein expressions, among other factors.

No mice except the DOX group and the GNPs&DOX-TL group over the course of this study showed neither any observable body weight loss nor any signs of toxicity such as diarrhea, neuropathy and edema (Fig. 13B). This strongly suggests that the liposome formulation could increase the biocompatibility of DOX and decrease the toxic effect to normal tissues. Besides, the GNPs&DOX-TLs showed more apparent weight loss than HGNPs&DOX-TLs which may be due to high EE inside the liposome. The enhanced antitumor efficiency for HGNPs&DOX-TLs with NIR laser irradiation can be attributed to several factors. First, the multifunctional HGNPs&DOX-TLs with the appropriate size could successfully permeate the tumors by the EPR effect. Second, the on-demand drug release from the HGNPs&DOX-TLs triggered by NIR laser irradiation disrupts the liposomal membrane and leads to local drug release, which increases the antitumor effects of DOX more effectively than GNPs&DOX-TLs. Third, the laser-caused hyperthermia can not only directly ablate tumor cells, but can also increase the cell membrane permeability and fluidity, thus promoting drug accumulation inside the cells. These results indicated that a combination strategy of chemotherapy and photothermal therapy would be a promising approach to effective antitumor therapy.

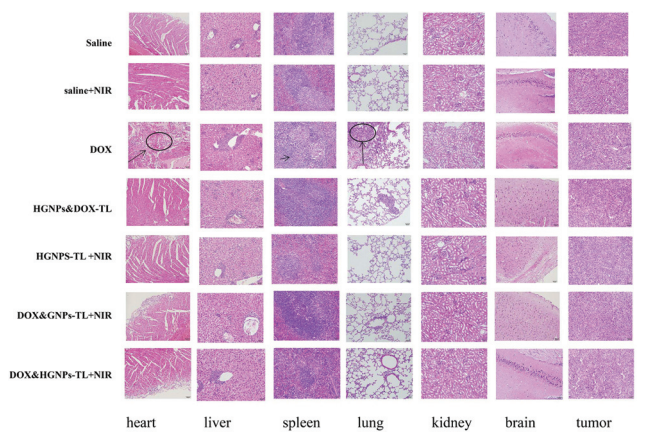

Fig. 14 Pathological examination of various tissue samples (heart, liver, spleen, lung, kidney, brain, and tumor) from MCF-7 tumor-bearing mice treated with saline, saline + NIR, DOX, HGNPs&DOX-TLs, HGNPs-TL + NIR, GNPs&DOX-TL + NIR and HGNPs&DOX-TL + NIR collected on the 30th day.

3.12 Systemic toxicity investigation

Pathological changes were evaluated using histological safety evaluation to further evaluate the safety of the HGNPs&DOX-TLs (Fig. 14). Compared with saline, no apparent signs of inflammatory response, cell degeneration or necrosis in major organs associated with long animal toxicity were observed during the HGNPs&DOX-TL treatment period, while there appeared an apparent inflammatory response in the heart tissue with DOX solution. This delivery system could decrease the side effect of DOX to the heart and achieve more significant anti-tumor efficiency as described above. These results were consistent with the weight changes which indicated the safety of HGNPs&DOX-TLs.

4. Conclusions

In summary, the highly reproducible and facile synthesis of 800 nm absorbing HGNPs using PVP as a cobalt template stabilizing agent with negligible cytotoxicity has been demonstrated in the present work. PVP most likely slows down the nucleation and the gold growth process, which makes it easier to produce thin shells that are necessary for generating SPR at desired NIR wavelengths for thermotherapy, particularly 800 nm. We then studied DOX&GNPs-TLs and DOX&HGNPs-TLs for their light to heat transduction efficiencies, *in vitro* cytotoxicity, intracellular uptake, and synergetic efficacy of chemotherapy and photothermal therapy under NIR laser irradiation. It was observed that DOX&GNPs-TLs are highly efficient light-to-heat transducers and require five times the mass of gold to cause an equivalent temperature rise at a given laser intensity when compared to DOX&HGNPs-TLs. Differences in *in vitro* drug release, cytotoxicity and intracellular uptake were observed for MCF-7 cells with DOX&HGNPs-TLs being taken up to a greater cytotoxicity than DOX&GNPs-TLs under NIR illumination. The DOX&HGNPs-TLs offered better therapeutically relevant heating capabilities and significant thermo-chemotherapy efficiency compared to DOX&GNPs-TLs. Overall, the prepared DOX&HGNPs-TLs simultaneously possessed an ideal size distribution, preferable photothermal-responsive locally drug release by disrupting the liposomal membrane, and excellent antitumor effects by achieving synergetic efficacy of chemotherapy and photothermal therapy under NIR laser irradiation. This strongly suggests that this multifunctional co-delivery system holds great promise for the development of a new antitumor treatment system.

Conflicts of interest

There are no conflicts to declare.

Acknowledgements

The authors would like to thank China Pharmaceutical University and Northeastern University for providing funding

and facilities. This work was funded by the National Natural Science Foundation of China (No. 81673364), the Ministry of Science and Technology of China (No. 2017ZX09101001-005-003), and College Students Innovation Project for the R&D of Novel Drugs (J1310032).

References

1 D. J. Wu, D. C. Wang, Y. F. Cheng, M. J. Qian, M. M. Zhang, Q. Shen and X. D. Wang, *Semin. Cancer Biol.*, 2017, **42**, 13–19.
2 S. Koren and M. Bentires-Alj, *Mol. Cell*, 2015, **60**, 537–546.
3 L. Vigano, L. Capussotti, G. De Rosa, W. O. De Saussure, G. Mentha and L. Rubbia-Brandt, *Ann. Surg.*, 2013, **258**, 731–740; discussion 741–732.
4 J. Held-Warmkessel, *Nursing*, 1998, **28**, 41–45; quiz 45–46.
5 J. T. Faught, P. A. Balter, J. L. Johnson, S. F. Kry, L. E. Court, F. C. Stingo and D. S. Followill, *Med. Phys.*, 2017, **44**, 5575–5583.
6 P. Leger, A. H. Limper and F. Maldonado, *Clin. Chest Med.*, 2017, **38**, 209–222.
7 S. L. Due, D. I. Watson, I. Bastian, G. Q. Ding, O. A. Sukocheva, D. S. Astill, L. Vat and D. J. Hussey, *Surg. Oncol.*, 2016, **25**, 269–277.
8 D. D. Lasic and N. S. Templeton, *Adv. Drug Delivery Rev.*, 1996, **20**, 221–266.
9 V. P. Torchilin, *Nat. Rev. Drug Discovery*, 2005, **4**, 145–160.
10 R. Mo, T. Y. Jiang, R. DiSanto, W. Y. Tai and Z. Gu, *Nat. Commun.*, 2014, **5**, 3364.
11 T. L. Andresen, S. S. Jensen and K. Jorgensen, *Prog. Lipid Res.*, 2005, **44**, 68–97.
12 Q. Y. Zhang, J. Tang, L. Fu, R. Ran, Y. Y. Liu, M. Q. Yuan and Q. He, *Biomaterials*, 2013, **34**, 7980–7993.
13 J. Davidsen, K. Jorgensen, T. L. Andresen and O. G. Mouritsen, *Biochim. Biophys. Acta, Biomembr.*, 2003, **1609**, 95–101.
14 J. Lu, E. Choi, F. Tamanoi and J. I. Zink, *Small*, 2008, **4**, 421–426.
15 A. Schroeder, R. Honen, K. Turjeman, A. Gabizon, J. Kost and Y. Barenholz, *J. Controlled Release*, 2009, **137**, 63–68.
16 K. J. Chen, H. F. Liang, H. L. Chen, Y. Wang, P. Y. Cheng, H. L. Liu, Y. Xia and H. W. Sung, *ACS Nano*, 2013, **7**, 438–446.
17 K. J. Chen, E. Y. Chaung, S. P. Wey, K. J. Lin, F. Cheng, C. C. Lin, H. L. Liu, H. W. Tseng, C. P. Liu, M. C. Wei, C. M. Liu and H. W. Sung, *ACS Nano*, 2014, **8**, 5105–5115.
18 S. Mura, J. Nicolas and P. Couvreur, *Nat. Mater.*, 2013, **12**, 991–1003.
19 X. Q. An, F. Zhan and Y. Y. Zhu, *Langmuir*, 2013, **29**, 1061–1068.
20 J. You, G. D. Zhang and C. Li, *ACS Nano*, 2010, **4**, 1033–1041.
21 E. Pastrana, *Nat. Methods*, 2012, **10**, 36–36.
22 G. Ajnai, A. Chiu, T. Kan, C.-C. Cheng, T.-H. Tsai and J. Chang, *J. Exp. Clin. Med.*, 2014, **6**, 172–178.
23 J. H. Park, G. von Maltzahn, M. J. Xu, V. Fogal, V. R. Kotamraju, E. Ruoslahti, S. N. Bhatia and M. J. Sailor, *Proc. Natl. Acad. Sci. U. S. A.*, 2010, **107**, 981–986.
24 Z. Xiao, C. Ji, J. Shi, E. M. Pridgen, J. Frieder, J. Wu and O. C. Farokhzad, *Angew. Chem., Int. Ed.*, 2012, **51**, 11853–11857.
25 S. Adams and J. Z. Zhang, *Coord. Chem. Rev.*, 2016, **320**, 18–37.
26 B. D. Chithrani, A. A. Ghazani and W. C. W. Chan, *Nano Lett.*, 2006, **6**, 662–668.
27 J. P. Yang, D. K. Shen, L. Zhou, W. Li, X. M. Li, C. Yao, R. Wang, A. M. El-Toni, F. Zhang and D. Y. Zhao, *Chem. Mater.*, 2013, **25**, 3030–3037.
28 S. Hong, K. Yang, B. Kang, C. Lee, I. T. Song, E. Byun, K. I. Park, S. W. Cho and H. Lee, *Adv. Funct. Mater.*, 2013, **23**, 1774–1780.
29 Y. H. Lee, H. Lee, Y. B. Kim, J. Y. Kim, T. Hyeon, H. Park, P. B. Messersmith and T. G. Park, *Adv. Mater.*, 2008, **20**, 4154–4157.
30 J. van der Zee, *Ann. Oncol.*, 2002, **13**, 1173–1184.
31 W. T. Al-Jamal and K. Kostarelos, *Acc. Chem. Res.*, 2011, **44**, 1094–1104.
32 H. Zhang, *Methods Mol. Biol.*, 2017, **1522**, 17–22.
33 S. Vemuri and C. T. Rhodes, *J. Pharm. Pharmacol.*, 1994, **46**, 778–783.
34 J. Fabrega, S. N. Luoma and C. R. Tyler, *Environ. Int.*, 2011, **37**, 517–531.
35 M. V. Bandulasena, G. T. Vladisavljevic, O. G. Odunmbaku and B. Benyahia, *Chem. Eng. Sci.*, 2017, **171**, 233–243.
36 E. Hao, S. Y. Li, R. C. Bailey, S. L. Zou, G. C. Schatz and J. T. Hupp, *J. Phys. Chem. B*, 2004, **108**, 1224–1229.
37 R. Suzuki, T. Takizawa, Y. Kuwata, M. Mutoh, N. Ishiguro, N. Utoguchi, A. Shinohara, M. Eriguchi, H. Yanagie and K. Maruyama, *Int. J. Pharm.*, 2008, **346**, 143–150.
38 A. M. Schwartzberg, T. Y. Olson, C. E. Talley and J. Z. Zhang, *J. Phys. Chem. B*, 2006, **110**, 19935–19944.
39 N. Zhang, H. Chen, A. Y. Liu, J. J. Shen, V. Shah, C. Zhang, J. Hong and Y. Ding, *Biomaterials*, 2016, **74**, 280–291.
40 E. Samuelsson, H. Shen, E. Blanco, M. Ferrari and J. Wolfram, *Colloids Surf., B*, 2017, **158**, 356–362.
41 J. Geng, C. Sun, J. Liu, L. D. Liao, Y. Yuan, N. Thakor, J. Wang and B. Liu, *Small*, 2015, **11**, 1603–1610.